Coherent dynamics and decoherence in a superconducting weak link

J. T. Peltonen,[1,*] Z. H. Peng,[1] Yu. P. Korneeva,[2] B. M. Voronov,[2] A. A. Korneev,[2,3,4] A. V. Semenov,[2,3] G. N. Gol'tsman,[2,4] J. S. Tsai,[1,5] and O. V. Astafiev[6,7,1,3,†]

[1] *RIKEN Center for Emergent Matter Science, Wako, Saitama 351-0198, Japan*
[2] *Moscow State Pedagogical University, 01069, Moscow, Russia*
[3] *Moscow Institute of Physics and Technology, 141700, Dolgoprudny, Moscow Region, Russia*
[4] *National Research University Higher School of Economics, Moscow Institute of Electronics and Mathematics, 109028, Moscow, Russia*
[5] *Department of Physics, Tokyo University of Science, Kagurazaka, Tokyo 162-8601, Japan*
[6] *Royal Holloway, University of London, Egham, Surrey TW20 0EX, United Kingdom*
[7] *National Physical Laboratory, Hampton Road, Teddington TW11 0LW, United Kingdom*

(Dated: July 25, 2016)

We demonstrate coherent dynamics of quantized magnetic fluxes in a superconducting loop with a weak link – a nanobridge patterned from the same thin NbN film as the loop. The bridge is a short rounded shape constriction, close to 10 nm long and 20 – 30 nm wide, having minimal width at its center. It superposes neighboring fluxoid states of the loop. Quantum state control and coherent oscillations in the driven time evolution of the tunnel-junctionless system are achieved. Decoherence and energy relaxation in the system are studied using a combination of microwave spectroscopy and direct time-domain techniques. The effective flux noise behavior suggests inductance fluctuations as a possible cause of the decoherence.

Introduction. A variety of different superconducting artificial quantum systems, successfully developed and studied over the last decade, rely on Josephson tunnel junctions of the Superconductor – Insulator – Superconductor (SIS) type (see, e.g., Refs. 1–4). Most devices contain aluminium – aluminium oxide junctions deposited by evaporation through a suspended resist mask, while more involved Nb–Al–AlOx junctions have been investigated as well[5]. A recently proposed and explored alternative approach to superconducting qubits is based on a new phenomenon – coherent quantum phase slips (CQPS) occurring in superconducting nanowires[6,7]. Such systems were first demonstrated in disordered InO_x[8], and we discovered similar behavior in nanowires patterned from thin disordered NbN and TiN films[9].

Main findings. In this work we realize a novel type of a tunnel barrier for magnetic fluxes based on a purposely-patterned weak link in a disordered superconductor, and study its coherent quantum dynamics, decoherence, and energy relaxation. We embed the nanobridge weak link in a superconducting loop, thereby forming a flux qubit where the neighboring fluxoid states of the loop are coherently superposed. In contrast to a nanowire with large length-to-width ratio, the tunneling energy of the weak link is mainly determined by a single amplitude through the narrowest point. This helps to avoid interference between different amplitudes (Aharonov–Casher effect) which may take place in nanowire-based qubits with multiple intrinsic weak links, as well as energy fluctuations due to random charge jumps in dielectrics[10]. Our study can yield further experimental insight on the question to what extent nanowires with nominally uniform cross-section are dominated by a single intrinsic weak link.

Probing the coherent dynamics in a weak link is interesting in light of the intense research on the classical dynamics and transport in these basic superconducting structures[11]. However, weak links in highly disordered superconducting films have not been extensively studied, and the theory is still emerging. Here we successfully demonstrate coherent flux tunneling dynamics through the weak link, together with quantum state control. We study the lithographically defined constrictions using the quantum two-level system as a tool for the first time, complementary to the standard dc transport approach. Furthermore, we report a systematic investigation of decoherence and find constraints on the decoherence mechanisms in the system. Quantum dynamics in various types of superconducting weak links is under active study, and has been only recently observed in direct time-domain measurements for atomic contacts[12,13] and semiconducting nanowire-based SNS junctions[14,15].

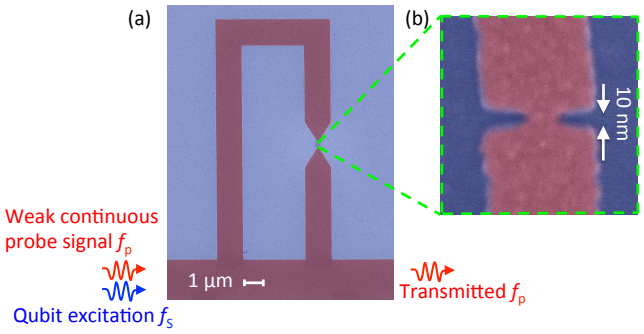

FIG. 1. (color online) (a) False color scanning electron micrograph of a typical NbN loop, interrupted by a narrow constriction. To control fluxes a perpendicular magnetic field B_{ext} is applied, producing a flux Φ_{ext} through the loop. The bottom edge of the loop is shared with the center conductor of a NbN coplanar waveguide resonator for microwave readout and control. (b) Enlarged view of the Dayem bridge type constriction between two 100 nm wide electrodes.

Figure 1 (b) shows a closeup of a typical constriction investigated in this work. As shown in Fig. 1 (a), the weak link is embedded into a superconducting loop and placed in a perpendicular magnetic field to realize the flux qubit. The qubit loop is coupled via shared kinetic inductance to a coplanar waveguide resonator that allows both microwave driving and probing of the qubit state. Each measured device contains several (up to 30) potential qubits coupled to the same readout resonator but with negligible direct coupling to each other due to the small mutual geometric inductance between the different loops. The multiplexed readout and control is an advantage of the resonator readout. On a larger scale, the sample structure is similar to Ref. 9.

The qubit loops have systematically different areas to allow reliable identification of a particular loop based on the magnetic field needed to produce one flux quantum. For a typical sample, microwave characterization reveals signatures originating from up to 5–10 qubits. Here we focus on one of the several measured chips, and present detailed measurements on one of the observed qubits, with the optimal point at $f_{\rm q} = 9.58$ GHz. The constriction lengths of the detected qubits were in the range $10 - 30$ nm, whereas the widths observed with a scanning electron microscope varied typically between 20 and 40 nm. In this limit of short electrode separations, due to the fabrication process, the nanobridge length and width are not independent of each other: the width typically decreases with increasing length. The fabrication yield is affected by our aim to minimize the length and width of the weak link: Both "shorted" (minimum width 100 nm corresponding to the electrode width) and broken (open loop) constrictions can occur. Moreover, the yield can not be directly accounted based on the microwave measurements alone: the qubits are on purpose made in such a way (by varying the nominal constriction width) that some of them are always outside of the measurement bandwidth.

Sample details. The samples are fabricated using a process similar to Ref. 9: First, a NbN film of thickness $d \approx 2 - 3$ nm is deposited on a Si substrate by DC reactive magnetron sputtering[16,17]. Proceeding with the uniform NbN film, a standard lift-off mask is patterned in a first round of electron beam lithography (EBL). This initial mask defines the coplanar resonator groundplanes as well as the transmission lines for connecting to the external microwave measurement circuit. These structures are subsequently metallized in an electron beam evaporator, followed by a standard lift-off process. In a second EBL step, the loops with constrictions as well as the resonator center line are patterned using a high-resolution negative resist (calixarene)[18–20]. Reactive ion etching (RIE) in CF_4 plasma is then used to finally transfer the pattern into the NbN film. The remaining resist is not removed after the etching process, which helps protecting the NbN structures against aging.

For electrical characterization of the samples, we employ a weak continuous microwave of frequency $f_{\rm p}$ as a probe signal and measure microwave transmission (normalized complex transmission coefficient $t = |t|e^{i\phi}$) through the resonator around one of the resonant modes using a vector network analyzer. The mode is chosen to fall within the usable $6 - 12$ GHz bandwidth of our cryogenic amplifier. We denote the probing power at the generator output by $P_{\rm p}$. As sketched in Fig. 1 (a), the qubit can be excited using a second, continuous or pulsed, microwave tone at frequency $f_{\rm s}$ and power $P_{\rm s}$. The resonator chip was enclosed in a sample box, and microwave characterization of the qubits was performed in a dilution refrigerator at the base temperature close to 25 mK.

The sample reported here contains a resonator with capacitive coupling. The resonant modes are given by $f_n = nv/(2L)$, $n = 1, 2, 3, \ldots$, where $L = 1.5$ mm is the resonator length, $v = 1/(L_l C_l)^{1/2}$ the effective speed of propagation of the electromagnetic waves, and L_l (C_l) the inductance (capacitance) per unit length. The qubit, shifted from the center of the resonator by about 100 μm, is coupled to several resonant modes, depending on the oscillating current amplitude. Transmission measurements yielded an average mode spacing of 2 GHz. We find $v \approx 6 \times 10^6$ m/s, and using the estimate $C_l \approx 1.0 \times 10^{-10}$ F/m we obtain $L_l \approx 2.8 \times 10^{-4}$ H/m, corresponding to the square inductance $L_\square \approx 1.4$ nH and characteristic impedance $Z_1 = (L_l/C_l)^{1/2} \approx 1.7$ kΩ. The full width at half maximum of the power transmission peak at $n = 6$ with frequency $f_6 = 11.876$ GHz (where the most of measurements are done) is $\Delta f_6 \approx 23$ MHz, which corresponds to a quality factor $Q \approx 500$. This value is partially limited by the internal quality factor $Q_{\rm int}$, typically of the same order as the coupling quality factor $Q_{\rm ext}$ for our devices. Using coplanar waveguide resonators to study the electrodynamics of disordered superconductors is an active top[21,22], and it will be interesting to extend the in-depth resonator studies to ultrathin NbN films similar to the one employed in our study.

Qubit characterization. We now demonstrate that the weak link coherently superposes neighboring fluxoid states of the loop. Microwave characterization of the resonators typically showed flux-periodic signatures originating from several of the loops coupled to the same readout resonator. At first, to identify which loops form functioning and detectable qubits, we probe the microwave transmission around multiple resonant modes as a function of $\Phi_{\rm ext}$ over several flux periods. As in Ref. 9, the loop area increases by a factor of 3 between the smallest and the largest loop.

The initial identification based on the flux-periodicity of the transmission is followed by two-tone spectroscopy centered around the optimal point of each qubit to extract the minimum energy gap Δ (the magnetic flux tunneling energy) and the persistent current $I_{\rm p}$ from the $\Phi_{\rm ext}$-dependence of the qubit transition. Figure 2 (a) shows a typical result of such a measurement: Microwave transmission through the resonator is monitored continuously at a fixed frequency $f_{\rm p}$ using a weak probe tone at one of the resonant modes. The qubit is si-

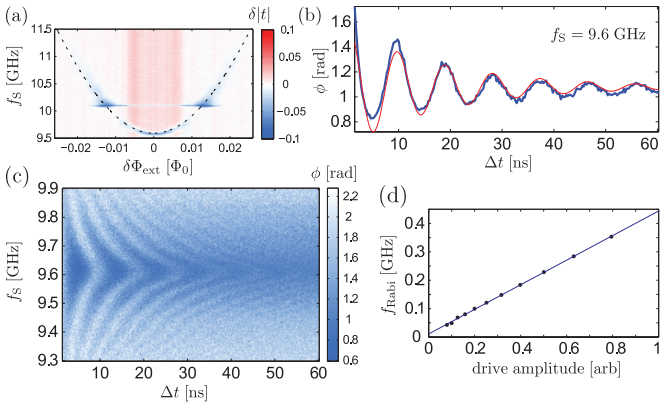

FIG. 2. (color online) (a) Two-tone spectroscopy of the system. The dashed line is a fit with $\Delta/h = 9.58$ GHz and $I_p = 40$ nA. The plot shows the change $\delta|t| = |t| - |t_0|$ in the magnitude of microwave transmission through the resonator. A f_s-independent reference signal $|t_0|$ due to the change of $|t|$ with Φ_{ext} at the probing frequency f_p has been subtracted for improved visualization. (b) Coherent oscillations close to the optimal point ($f_s = \Delta/h$), measured by changing the pulse length Δt of the pulsed, resonant microwave drive. The shown phase is the measured average phase when the system is continuously probed and the excitation pulse is repeated at intervals of $T = 500$ ns ($\gg T_1$, the energy relaxation time). The thin red line shows a fit to a decaying sinusoidal. (c) Rabi oscillations close to the optimal point, for a range of driving frequencies f_s. The trace in panel (b) corresponds to a line cut of a similar plot. (d) Dependence of Rabi frequency on the driving amplitude, showing linear increase towards stronger driving as evidence of the two-level nature of the system.

multaneously excited using a stronger drive tone at a frequency f_s that is scanned around f_q. Due to the dispersive (non-resonant) coupling between the qubit and the resonator, the resonant frequency depends on the qubit state populations. The populations ultimately saturate to 0.5 for strong drive, producing a clear dip in the measured transmission whenever $f_s = f_q$. In Fig. 2 (a) we plot the magnitude of the microwave transmission coefficient as a function of f_s and Φ_{ext}. The dashed line is a fit to $hf_q = \sqrt{\varepsilon^2 + \Delta^2}$, based on the Hamiltonian $H = -(\varepsilon/2)\sigma_z - (\Delta/2)\sigma_x$. Here, $\varepsilon = 2I_p\delta\Phi_{ext}$ with $\delta\Phi_{ext} = \Phi_{ext} - (N + 1/2)\Phi_0$, and $\Phi_0 = h/(2e)$ denotes the magnetic flux quantum. N labels the fluxoid state of the loop. In the vicinity of the point $\delta\Phi_{ext} = 0$, where the transition frequency f_q reaches its minimum value Δ/h, the fluxes are superposed. The dashed curve uses $I_p = 40$ nA, which is defined by the loop inductance $L_q = \Phi_0/(2I_p) \approx 25$ nH. The curve is a good approximation to the level spacing over our measurement bandwidth, up to $f_q \approx 20$ GHz. The probing frequency f_p, low excitation power P_s, and the color scale for the spectroscopy in Fig. 2 (a) were optimized for $f_q \approx \Delta/h$.

After spectroscopic characterization we perform direct time-domain probing with Φ_{ext} tuned to the optimal point, where $f_q = \Delta/h$. Figure 2 (c) shows the second main finding of this work: Using a pulsed microwave drive at frequency f_s close to f_q, and of varying duration Δt, we observe Rabi oscillations of the qubit population. To obtain this result, we keep the weak continuous probing tone at f_p, and the driving pulses of length Δt are repeated with period $T = 500$ ns. Figure 2 (b) shows a line cut at zero detuning, $f_s = f_q$, whereas Fig. 2 (d) illustrates good agreement between the observed oscillation frequencies at different driving powers and the characteristic linear dependence on the drive amplitude expected for a two level system. The oscillations decay here within about 30 ns. Besides the decaying oscillations, we typically observe a slow decay or increase of the background level. This happens over a larger range of Δt, often beyond 100 ns when the oscillations have already become undetectable. One of the possible causes is influence of the excitation pulses on the resonator transmission.

The time-domain oscillation measurements were performed at probing powers P_p corresponding to intraresonator photon numbers $n \lesssim 1$. To characterize the influence of the continuous measurement on the qubit dephasing we check the lineshape of the spectroscopy line at the qubit optimal point at varying probing powers. The observed negative ac-Stark shift of the qubit frequency, approximately linear with an increase of the readout power, allowed us to calibrate n against P_p as with aluminium-based superconducting qubits[23,24]. Due to the measurement backaction, at increasing P_p we observe the expected broadening of the spectroscopy line and the start of the evolution of its shape from a Lorentzian towards an inhomogeneously broadened Gaussian as the qubit transition frequency is affected by the instantaneous photon population in the resonator[23].

Decoherence measurements. Our earlier experiments with two-level systems in InO_x and NbN nanowires[8,9] indicated dephasing in these systems, with typical spectroscopy linewidths of the order of 100 MHz, but the decoherence properties were not investigated in detail. Figure 3 collects together the next finding of this work: measurements of dephasing and relaxation rates of the constriction qubit.

First, Fig. 3 (a) displays the spectroscopy line of the qubit when Φ_{ext} is kept fixed at the optimal point. The probing power P_p corresponds to $n \lesssim 1$ photons in the resonator on average, and the magnitude of the normalized transmission coefficient is plotted as a function of f_s. The lineshape is well described by a Lorentzian dip whose width and depth increase with P_s. In the limit of low P_s we find a full width at half maximum of $\delta f_{FWHM} = 26$ MHz at the optimal point, corresponding to a dephasing rate $\Gamma_2 = \pi\delta f_{FWHM} \approx 8 \times 10^7$ s^{-1}.

The dependence of Γ_2 on the qubit frequency f_q is shown in Fig. 3 (c), in the main panel in terms of ε over a wide range of the external flux, and in the inset in more detail around the optimal point. As evident already from Fig. 2 (a), the dephasing rates increase quickly when Φ_{ext} is moved away from the optimal point. The black solid line as an eye-guide is $2.9|\varepsilon|/(\hbar\omega_q)\times 10^9$ s^{-1}, the expected

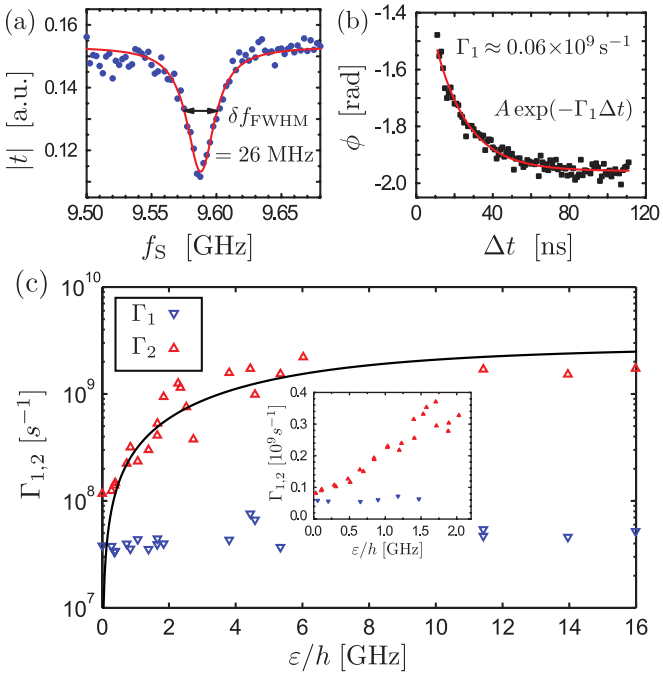

FIG. 3. (color online) (a) Typical spectroscopy lineshape of the qubit close to the optimal point (filled circles). The probing power $P_{\rm p}$ was kept constant at a low value corresponding to $n \lesssim 1$ photons in the readout resonator, in which case the measured signal is well described by a Lorentzian dip (red solid line), the width of which relates directly to the total decoherence rate $\Gamma_2 = \pi\delta f_{\rm FWHM}$. (b) Determination of the energy relaxation rate Γ_1 from exponential decay of the averaged transmission under repetitive driving with double pulses of constant length but varying delay Δt between the pulses. (c) Relaxation rates Γ_1 (downward blue/dark triangles) and total decoherence rates Γ_2 (upward red/light triangles) as a function of the energy bias ε. The solid line shows $2.9|\varepsilon|/(\hbar\omega_{\rm q}) \times 10^9$ s^{-1}. The inset plots Γ_1 and Γ_2 from another, more detailed measurement focused around the optimal point.

ε-dependence for $1/f$ type flux noise[25]. In Fig. 3 (c) we also show the energy relaxation rates $\Gamma_1 = 1/T_1$ as a function of the external magnetic flux. To reduce the effects of spurious excitations of nearby resonator modes, the qubit relaxation rates were obtained from exponential fits to a time domain measurement with two microwave pulses of fixed length 100 ns $\gg T_2$ whose separation was varied. The method is essentially the same as employed in Ref. 26, except that the π pulses are replaced by pulses much longer than T_2 and therefore they saturate the state populations to 50%. Figure 3 (b) displays a typical result. Similar to the measurements of the Rabi oscillations, the system was probed continuously at $f_{\rm p}$ and the pulse sequence was repeated after every $T = 500$ ns. In contrast to the dephasing rate that quickly increases away from the qubit optimal point, we find the relaxation rate corresponding to $T_1 \approx 30$ ns to be only weakly dependent on $\Phi_{\rm ext}$. Note also that the relaxation can not be described by the Purcell effect due to non-resonant energy leak to the resonator modes. This is supported by our estimates and frequency-independent behavior of Γ_1 when the qubit is detuned from the resonances, as is, for instance, shown in the inset of Fig. 3 (c).

Discussions. The increase of the dephasing rate in Fig. 3 (c) with increasing ε suggests that it originates from low frequency fluctuations in the flux degree of freedom. From the asymptotic relation $2I_{\rm p}\delta\Phi = 2\hbar\Gamma_2$ (at $\hbar\omega_{\rm q} \gg \Delta$, where $\Gamma_2 \approx 2.9 \times 10^9$ s^{-1}), we find the corresponding normalized flux fluctuations $\delta\Phi/\Phi_0$ to be about 4×10^{-3}, which is about three orders of magnitude larger than typical flux fluctuations in Josephson flux qubits and dc SQUIDs fabricated from thicker films[25,27–31]. The corresponding inductance fluctuations from $\delta\Phi/\Phi_0 = \delta L_{\rm q}/L_{\rm q}$ are found to be $\delta L_{\rm q} \approx 0.1$ nH. If we assume that the fluctuations are correlated in space with a typical characteristic length (e.g. coherence length) then the relative inductance fluctuations $\delta L_{\rm q}/L_{\rm q}$ are scaled as inverse square root of the total area. Recalculated for the resonator, we find that $\delta L_{\rm r}/L_{\rm r} = \sqrt{A_{\rm q}/A_{\rm r}}\delta L_{\rm q}/L_{\rm q} \approx 2.5 \times 10^{-4}$, where $A_{\rm q}$ and $A_{\rm r}$ are areas of the qubit and the resonator central line. If similar inductance fluctuations take place in the resonator formed from the same NbN film, the expected relative inductance fluctuations result in the resonator line broadening $\delta f = 1/2(f_n/2)\delta L_{\rm r}/L_{\rm r}$, which for f_6 is equal to 0.8 MHz. This is an order of magnitude smaller than the line broadening in our resonator Δf_6.

To deepen the understanding of decoherence by the effective flux fluctuations in these systems, it would be interesting to study similar weak links in films of different thicknesses, as this will strongly affect the degree of disorder. Likewise, the area of the film in the qubit loop can be varied and what is more, possible contact issues aside, part of the qubit loop could be fabricated from a thicker film.

Next, we characterize the qubit dissipation, assuming that it is caused by a resistance $R_{\rm q}$ parallel to the inductance. The relaxation rate caused by the spontaneous emission due to the current quantum noise $S_I(\omega_{\rm q}) = 2\hbar\omega_{\rm q}/(2\pi R_{\rm q})$ is $\Gamma_1 = 2\pi S_I(\omega_{\rm q})\varphi_{\rm p}^2 \sin^2\theta/\hbar^2$, where $\varphi_{\rm p} = L_{\rm q}I_{\rm p} = \Phi_0/2$ is the effective dipole moment, describing coupling of the loop to the resistance, and $\sin\theta = \Delta/\hbar\omega_{\rm q}$. Note that $\sin\theta$ changes only by a factor of 2 in the range of our measurements 9.58 GHz $\le f_{\rm q} \le$ 18 GHz (corresponding to $0 \le \varepsilon \le 16$ GHz), and Γ_1 fluctuates in a relatively narrow window over the measured frequency range. Although $R_{\rm q}$ is not necessarily constant, we estimate its effective value, substituting typical Γ_1. At $f_{\rm q} \approx 9.6$ GHz, $\Gamma_1 \approx 4 \times 10^7$ s^{-1}, and we find $R_{\rm q} \approx 30$ MΩ, which corresponds to a square resistance $R_\square \approx 1.7$ MΩ. The resistance is too large to explain the resonator quality factor, which due to the internal loss on a resistance parallel to the inductance would be $Q_{\rm R} = R_\square/(2\omega L_\square) \sim 10^4$. The nature of this dissipation requires further study. A possible mechanism can be related to crowding of the current part out of superconducting channel to a normal one (e.g., quasiparticle current or dissipative displace-

ment current in the oxide layer on top of the film) due to fluctuations of kinetic inductance.

Conclusions. To summarize, we have demonstrated coherent quantum dynamics in a superconducting loop interrupted by a weak link in the geometry of a uniform-thickness Dayem bridge type constriction. Quantum state control of the qubit has been demonstrated by measuring Rabi oscillations. The dephasing and energy relaxation have been studied in a wide range of energies. The dephasing can be explained by kinetic inductance fluctuations in the highly disordered NbN film. Future samples would benefit from a readout resonator with significantly larger fundamental frequency, better quality resonators fabricated in a separate step, as well as the loops fabricated from a thicker film. A detailed study of the constriction length dependence could shed light onto the transition to a phase slip flux qubit in a longer nanowire, either uniform or behaving as a chain of intrinsic weak links.

ACKNOWLEDGMENTS

The work was financially supported by the JSPS FIRST and ImPACT programs, MEXT Kakenhi 'Quantum Cybernetics', Royal Society within International Exchanges Scheme (2015 Russia RFBR #15-52-10044 KO_a Cost share), and Russian Scientific Fund (N 15-12-30030). J. T. P. acknowledges support from Academy of Finland (Contract No. 275167).

* joonas.peltonen@riken.jp; Present Address: Low Temperature Laboratory, Aalto University School of Science, POB 13500, FI-00076 AALTO, Finland

† Oleg.Astafiev@rhul.ac.uk

[1] M. H. Devoret and R. J. Schoelkopf, Science **339**, 1169 (2013).

[2] H. Paik, D. I. Schuster, Lev S. Bishop, G. Kirchmair, G. Catelani, A. P. Sears, B. R. Johnson, M. J. Reagor, L. Frunzio, L. I. Glazman, S. M. Girvin, M. H. Devoret, and R. J. Schoelkopf, Phys. Rev. Lett. **107**, 240501 (2011).

[3] R. Barends *et al.*, Nature **508**, 500 (2014).

[4] J. M. Chow, J. M. Gambetta, E. Magesan, S. J. Srinivasan, A. W. Cross, D. W. Abraham, N. A. Masluk, B. R. Johnson, C. A. Ryan, and M. Steffen, Nat. Comm. **5**, 4015 (2014).

[5] D. A. Bennett, L. Longobardi, V. Patel, W. Chen, D. V. Averin, and J. E. Lukens, Quant. Inf. Proc. **8**, 217 (2009).

[6] J. E. Mooij and C. J. P. M. Harmans, N. J. Phys. **7**, 219 (2005).

[7] J. E. Mooij and Yu. V. Nazarov, Nat. Phys. **2**, 169 (2006).

[8] O. V. Astafiev, L. B. Ioffe, S. Kafanov, Yu. A. Pashkin, K. Yu. Arutyunov, D. Shahar, O. Cohen, and J. S. Tsai, Nature **484**, 355 (2012).

[9] J. T. Peltonen, O. V. Astafiev, Yu. P. Korneeva, B. M. Voronov, A. A. Korneev, I. M. Charaev, A. V. Semenov, G. N. Gol'tsman, L. B. Ioffe, T. M. Klapwijk, and J. S. Tsai, Phys. Rev. B **88**, 220506(R) (2013).

[10] M. Vanevic and Yu. V. Nazarov, Phys. Rev. Lett. **108**, 187002 (2012).

[11] K. K. Likharev, Rev. Mod. Phys. **51**, 101 (1979).

[12] C. Janvier, L. Tosi, L. Bretheau, Ç. Ö. Girit, M. Stern, P. Bertet, P. Joyez, D. Vion, D. Esteve, M. F. Goffman, H. Pothier, and C. Urbina, Science **349**, 1199 (2015).

[13] C. Janvier, L. Tosi, Ç. Ö. Girit, M. F. Goffman, H. Pothier, and C. Urbina, J. Phys.: Condens. Matter **26**, 474208 (2014).

[14] T. W. Larsen, K. D. Petersson, F. Kuemmeth, T. S. Jespersen, P. Krogstrup, J. Nygard, C. M. Marcus, Phys. Rev. Lett. **115**, 127001 (2015).

[15] G. de Lange, B. van Heck, A. Bruno, D. J. van Woerkom, A. Geresdi, S. R. Plissard, E. P. A. M. Bakkers, A. R. Akhmerov, and L. DiCarlo, Phys. Rev. Lett. **115**, 127002 (2015).

[16] G. N. Gol'tsman, K. Smirnov, P. Kouminov, B. Voronov, N. Kaurova, V. Drakinsky, J. Zhang, A. Verevkin, and R. Sobolewski, IEEE Trans. Appl. Supercond. **13**, 192 (2003).

[17] A. Korneev, Yu. Korneeva, I. Florya, B. Voronov, and G. Gol'tsman, Proc. SPIE **8072**, 80720G (2011).

[18] Commercially available as 'TEBN-1' from Tokuyama Corporation, www.tokuyama.co.jp.

[19] J. Fujita, Y. Ohnishi, Y. Ochiai, and S. Matsui, Appl. Phys. Lett. **68**, 1297 (1996).

[20] M. Narihiro, K. Arai, M. Ishida, Y. Ochiai, and Y. Natsuka, Jpn. J. Appl. Phys. **44**, 5581 (2005).

[21] P. C. J. J. Coumou, E. F. C. Driessen, J. Bueno, C. Chapelier, and T. M. Klapwijk, Phys. Rev. B **88**, 180505(R) (2013).

[22] M. Zemlicka, P. Neilinger, M. Trgala, M. Rehák, D. Manca, M. Grajcar, P. Szabó, P. Samuely, S. Gazi, U. Hübner, V. M. Vinokur, and E. Il'ichev, Phys. Rev. B **92**, 224506 (2015).

[23] D. I. Schuster, A. Wallraff, A. Blais, L. Frunzio, R.-S. Huang, J. Majer, S. M. Girvin, and R. J. Schoelkopf, Phys. Rev. Lett. **94**, 123602 (2005).

[24] A. A. Abdumalikov, Jr., O. V. Astafiev, Y. Nakamura, Y. A. Pashkin, and J. S. Tsai, Phys. Rev. B **78**, 180502(R) (2008).

[25] F. Yoshihara, K. Harrabi, A. O. Niskanen, Y. Nakamura, and J. S. Tsai, Phys. Rev. Lett. **97**, 167001 (2006).

[26] A. A. Abdumalikov, Jr., O. V. Astafiev, Yu. A. Pashkin, Y. Nakamura, and J. S. Tsai, Phys. Rev. Lett. **107**, 043604 (2011).

[27] F. Yan, J. Bylander, S. Gustavsson, F. Yoshihara, K. Harrabi, D. G. Cory, T. P. Orlando, Y. Nakamura, J. S. Tsai, and W. D. Oliver, Phys. Rev. B **85**, 174521 (2012).

[28] M. Stern, G. Catelani, Y. Kubo, C. Grezes, A. Bienfait, D. Vion, D. Esteve, and P. Bertet, Phys. Rev. Lett. **113**, 123601 (2014).

[29] J.-L. Orgiazzi, C. Deng, D. Layden, R. Marchildon, F. Kitapli, F. Shen, M. Bal, F. R. Ong, and A. Lupascu, arXiv:1407.1346 (2014).

[30] S. M. Anton, J. S. Birenbaum, S. R. OKelley, V. Bolkhovsky, D. A. Braje, G. Fitch, M. Neeley, G. C. Hilton, H.-M. Cho, K. D. Irwin, F. C. Wellstood, W. D. Oliver,

A. Shnirman, and J. Clarke, Phys. Rev. Lett. **110**, 147002 (2013).

[31] F. Yan, S. Gustavsson, A. Kamal, J. Birenbaum, A. P. Sears, D. Hover, T. J. Gudmundsen, J. L. Yoder, T. P. Orlando, J. Clarke, A. J. Kerman, and W. D. Oliver, arXiv:1508.06299 (2015).